Zhu *et al. Microstructures* **2025**, *5*, 2025040
DOI: 10.20517/microstructures.2024.108

Microstructures

Research Article

Open Access

Check for updates

Preparation of Co_3S_4/rGO composites and their supercapacitor performances

Mingxing Zhu[1], Xinlei Han[1], Kaiming Zhang[1], Huan Liu[2], Chunyu Li[1], Hongru Sun[1], Qing Wen[2,3], Jing Zhao[2,3], Guiling Wang[2,3]

[1]Heilongjiang Longxing International Resources Development Group Co., Ltd. Harbin 150036, Heilongjiang, China.
[2]Key Laboratory of Superlight Materials and Surface Technology of Ministry of Education, College of Materials Science and Chemical Engineering, Harbin Engineering University, Harbin 150001, Heilongjiang, China.
[3]Heilongjiang Hachuan Carbon Materials Technology Co., LTD, National Quality Supervision and Inspection Center of Graphite Productst, Jixi 158100, Heilongjiang, China.

Correspondence to: Prof. Guiling Wang and Dr. Jing Zhao, Key Laboratory of Superlight Materials and Surface Technology of Ministry of Education, College of Materials Science and Chemical Engineering, Harbin Engineering University, No. 145 Nantong Street, Harbin 150001, Heilongjiang, China. E-mail: wangguiling@hrbeu.edu.cn; E-mail: zhtdzhn@163.com

How to cite this article: Zhu, M.; Han, X.; Zhang, K.; Liu, H.; Li, C.; Sun, H.; Wen, Q.; Zhao, J.; Wang, G. Preparation of Co_3S_4/rGO composites and their supercapacitor performances. *Microstructures* **2025**, *5*, 2025040. https://dx.doi.org/10.20517/microstructures.2024.108

Received: 30 Oct 2024 **First Decision:** 10 Dec 2024 **Revised:** 3 Jan 2025 **Accepted:** 8 Jan 2025 **Published:** 15 Apr 2025

Academic Editors: Shujun Zhang, Zonghoon Lee **Copy Editor:** Shuyuan Duan **Production Editor:** Shuyuan Duan

Abstract

Graphene, with its two-dimensional structure, offers high mechanical flexibility and excellent conductivity, but its tendency to stack and aggregate in practical applications reduces the effective surface area, resulting in rapid capacity degradation. To overcome this, we in situ grow rod-like Co_3S_4 structures on graphene oxide graphene oxide (rGO), forming a highly conductive and mechanically stable composite. The Co_3S_4 nanoparticles serve as active sites for redox reactions, significantly improving the specific capacitance, while the rGO matrix enhances electron transport and mitigates the issues of volume expansion during charge/discharge cycles. The Co_3S_4/rGO composite is synthesized via a two-step hydrothermal process, and the effects of sulfuration temperature and time on electrochemical performance are systematically explored. The results show that the Co_3S_4/rGO-160-8 composite, synthesized at 160 °C for eight hours, achieves a specific capacitance of 1442.5 $F \cdot g^{-1}$ at 1 $A \cdot g^{-1}$ and exhibits a capacity retention of 93.3% after 5000 cycles at 4 $A \cdot g^{-1}$. Furthermore, the Co_3S_4/rGO-160-8//activated carbon asymmetric supercapacitor delivers an energy density of 47.0 $Wh \cdot kg^{-1}$ at 749.8 $W \cdot kg^{-1}$ power density, with only an 8.9% capacity loss after 5000 cycles, demonstrating excellent cycling stability. This novel composite material offers a promising approach for high-performance supercapacitors, balancing high energy density, excellent rate performance, and long-term stability.

Keywords: Co_3S_4, supercapacitor, electrochemical performance, composite materials

INTRODUCTION

With the escalating global energy crisis and environmental challenges, the development and utilization of energy have become significant topics in today's world[1]. Consequently, the search for sustainable, environmentally friendly, and efficient energy storage devices has emerged as a critical area of research. Currently, energy storage devices primarily include supercapacitors, batteries, and fuel cells[2]. Among these, supercapacitors, as an emerging energy storage technology, demonstrate significant potential across diverse fields, such as portable electronics, electric vehicles, medical devices, and aerospace, due to their high power density, fast charge-discharge capability and extended lifespan. However, their relatively lower energy density compared to batteries constrains further advancements in supercapacitor technology. Therefore, recent research has focused on enhancing energy density without compromising the high power density and long cycle life of supercapacitors[3].

Electrode materials are essential to the energy storage performance of supercapacitors. Researchers have been dedicated to developing new electrode materials to optimize supercapacitor performance[4]. By rationally designing the structure and composition of electrode materials, the specific surface area and capacitance of electrodes can be improved, thus increasing the energy density of supercapacitors. Graphene, as a novel carbon nanomaterial, is widely applied in supercapacitor electrodes due to its high specific surface area and excellent conductivity[5,6]. However, in supercapacitor applications, graphene's layered stacking characteristics can reduce its specific surface area and electrochemical activity[7]. To overcome this drawback, the combination of transition metal oxides and sulfides with graphene as electrode materials has been explored. This not only effectively prevents graphene from stacking but also significantly enhances the overall capacitance performance of the composite materials[8]. By complementing each other's advantages, the issues of insufficient stability of transition metal compounds and the limited capacitance of graphene can be effectively alleviated, thereby greatly improving the overall performance and application prospects of supercapacitors.

Transition metal sulfides, particularly Co_xS_y, are promising candidates for enhancing the energy density of supercapacitors due to their high theoretical specific capacitance, stemming from their redox capabilities and multiple oxidation states. Materials such as MnO_2, Fe_3O_4, NiO, and Co_3O_4 have garnered attention due to their low cost and potential electrochemical performance[9]. Compared to their corresponding oxides, transition metal sulfides exhibit better conductivity, thermal stability, and redox activity[10]. When choosing the less electronegative sulfur (S) to replace oxygen (O), a more resilient structure can be formed, reducing structural collapse while retaining high stability. Additionally, the presence of multiple valence states in transition metal sulfides increases the number of electrons participating in the redox reactions during charge-discharge processes, providing higher capacitance. Cobalt sulfide (Co_xS_y) comprises cobalt and sulfur in various stoichiometric ratios, including CoS, CoS_2, Co_3S_4, and Co_9S_8[11]. Cobalt sulfides, characterized by low electronegativity, unique crystal structures, and high theoretical capacitance values, have been employed as electrode materials for supercapacitors. For instance, Hu *et al.* synthesized hollow nanoboxes assembled from CoS nanoparticles starting from cobalt-based zeolitic imidazolate frameworks (ZIF-67). This hollow structure features a high specific surface area and rich pore distribution, enhancing electrolyte transport and providing more active sites for electrochemical reactions, achieving a capacitance of 980 $F \cdot g^{-1}$. Zhou *et al.* prepared Co_9S_8 nanosheets anchored carbon cloth (CC) via a two-step hydrothermal method. Owing to the conductive CC substrate and the distinctive multi-layered micro/nanostructure of Co_9S_8[12]. The flexible Co_9S_8/CC electrode preserves its electrochemical integrity under mechanical deformation, such as bending and twisting. It achieves a specific capacitance of 1475.4 $F \cdot g^{-1}$ at a current density of 1 $A \cdot g^{-1}$, demonstrates an excellent rate capability with 80.2% retention at 20 $A \cdot g^{-1}$, and exhibits superior cycling stability, maintaining

92.9% capacitance retention after 5000 cycles. However, the application of Co_xS_y materials is limited by their poor electrical conductivity and mechanical instability.

Three-dimensional graphene, as a special carbon material with an extremely high specific surface area, has a network-like structure of single-layer carbon atoms that is suitable for use as a substrate or connecting material. Therefore, the incorporation of graphene enhances the conductivity of the material. The oxygen-containing groups present facilitate the nucleation and growth of metal precursors, promoting the uniform distribution of sulfides and increasing the specific surface area of materials[13]. The conductive network formed by graphene not only accelerates charge transfer rates but also reduces the agglomeration of sulfides, alleviating volume changes and significantly improving the electrochemical performances of the electrodes. Yang *et al.*[14] successfully anchored NiS nanorods onto graphene sheets via a two-step hydrothermal method, forming a three-dimensional conductive network that accelerates electron transfer rates, achieving a specific capacitance of 905.3 $F \cdot g^{-1}$ at 1 $A \cdot g^{-1}$.

This work prepared Co_3S_4 nanoparticles on reduced graphene oxide (rGO) sheets through a two-step hydrothermal process, forming a highly conductive and mechanically stable composite material. The Co_3S_4 nanoparticles, serving as active sites for redox reactions, significantly enhance the specific capacitance, while the integration with rGO, known for its excellent conductivity and mechanical strength, ensures efficient electron transport and mitigates issues related to volume expansion during charge/discharge cycles. This novel rGO-Co_3S_4 composite material demonstrates excellent rate performance, high energy density, and improved cycling stability, making it a promising candidate for high-performance supercapacitors without sacrificing power density. The results present that the electrochemical performance of the synthesized Co_3S_4 /rGO-160-8 electrode material is optimal, achieving a mass-specific capacitance of 1442.5 $F \cdot g^{-1}$ at a current density of 1 $A \cdot g^{-1}$. The synergistic effect between the two components endows the composite material with outstanding cycling stability, with only a 6.7% capacity degradation after 5000 cycles at 4 $A \cdot g^{-1}$. When used as the positive electrode to construct a Co_3S_4/rGO-160-8//AC asymmetric supercapacitor, it attains an energy density of 47.0 $Wh \cdot kg^{-1}$ at a power density of 749.8 $W \cdot kg^{-1}$. Moreover, following 5000 charge-discharge cycles at a current density of 4 $A \cdot g^{-1}$, it demonstrates a capacity retention of 91.1%, indicative of its exceptional cycling stability.

MATERIALS AND METHODS

Raw materials

The raw materials of graphene oxide (GO) used in this paper were purchased from CNBM Heilongjiang Graphite New Materials Co., Ltd. and the $CoCl_2 \cdot 6H_2O$, NH_4F and urea were analytically pure and purchased from Tianjin Kemeiou Chemical Reagents Co., Ltd.

Preparation of Co_3S_4/rGO composites

First, 40 mg of GO powder was added to 30 mL of deionized water and subjected to ultrasonic treatment for one hour to achieve a homogeneous dispersion, resulting in a uniformly colored brown suspension. Sequentially, 2.0 mmol of $CoCl_2 \cdot 6H_2O$, 5.0 mmol of NH_4F, and 6.0 mmol of urea were added to the suspension, followed by magnetic stirring for 10 min to ensure uniform mixing. The resulting solution was then transferred to a 50 mL reaction vessel, which was placed in an oven and heated to 90 °C for 10 h. After cooling the reaction vessel to room temperature, the reaction solution was filtered through a funnel, and the powder on the filter paper was subjected to freeze-drying.

Then, 60 mg of the aforementioned precursor was mixed with 30 mL of $Na_2S \cdot 9H_2O$ (0.2 $mol \cdot L^{-1}$) solution and stirred for 30 min before transferring it to a 50 mL reaction vessel. The vessel was heated to a specified

temperature in the oven and maintained for a set duration. Following cooling to room temperature, the mixture underwent filtration and was subsequently rinsed with deionized water, and the resulting black powder on the filter paper was freeze-dried. This investigation seeks to elucidate the effects of sulfuration temperature and duration on the electrochemical performance characteristics of supercapacitors; the naming convention was established as Co_3S_4/rGO-temperature-time. Co_3S_4 electrode materials were prepared without the addition of graphene at sulfuration conditions of 160 °C and 8 h.

Characterization and testing methods

X-ray diffraction (XRD) was used to analyze the material's crystalline structure and phase composition (D/max-TTR^{III}, Rigaku Corporation, Japan). Scanning electron microscopy (SEM) employs a focused high-speed electron beam to scan the sample surface, producing secondary electron images that reveal its microscopic morphology (JSM-6480A). An Energy Dispersive X-ray Spectrometer (EDS) can be coupled to SEM to analyze the elemental composition based on the characteristic X-ray wavelengths emitted by different elements. Transmission electron microscopy (TEM) was primarily used to observe the material's microstructure and crystalline orientation (FeiTecnia G2-STWIN, Philips, Netherlands). X-ray photoelectron spectroscopy (XPS) analyzes the elemental composition, valence states, and chemical bonds on the material's surface (ESCALAB 250, Thermo Fisher Scientific Co., Ltd., China). XPS tested with an Al anode, a spot size of 500 μm, a step size of 0.05 eV, and a pass energy of 30 eV. Raman spectroscopy provides insights into molecular vibrations and rotations, aiding in the structural determination of compounds (HR800 manufactured by Jobin Yvon, France). Thermogravimetric analysis (TGA) is a thermal analysis technique that studies changes in a material's mass as a function of temperature. This method allows for the assessment of thermal stability and decomposition behavior (TGADSC^{3+}, TA Instruments, USA).

Characterizations of electrochemical performances

The electrode preparation process was conducted as follows: a piece of nickel foam measuring 1.2 cm × 1.2 cm was first immersed in acetone and then in a 1.5 mol·L^{-1} hydrochloric acid solution for ten minutes with ultrasonic treatment. The foam was subsequently rinsed with water and ethanol to remove any grease and oxides from its surface. Five milligrams of active material [or activated carbon (AC)] and 0.5 mg of conductive carbon black were weighed, and then mixed with 16 μL of 5% Nafion, 0.25 mL of deionized water, and 0.25 mL of ethanol to form a homogenous solution through 10 min of ultrasonic treatment. This final solution was then drop-coated onto the nickel foam.

In this study, a three-electrode testing configuration was utilized to assess the performance of the synthesized supercapacitor electrodes. The nickel foam, which was loaded with the active material, served as the working electrode, while a carbon rod functioned as the counter electrode, and an Ag/AgCl electrode was employed as the reference. To evaluate the practical applicability of the fabricated electrodes, an asymmetric supercapacitor was assembled, incorporating the prepared electrode as the positive terminal and an AC electrode as the negative terminal, with a cellulose membrane acting as the separator. Both the three-electrode and two-electrode testing setups utilized a 6 M KOH solution as the electrolyte. Cyclic voltammetry (CV) and galvanostatic charge-discharge (GCD) electrochemical impedance spectroscopy (EIS) characterizations of the electrode materials were performed at room temperature using an electrochemical workstation.

The device's power and energy density can be calculated using the specific capacitance. This method can also assess the cycling performance of the material. The specific capacitance of the electrode material during charge-discharge cycles can be calculated using

$$C_m = \frac{I \times \Delta t}{\Delta V \times m} \quad (1)$$

where Cm ($F \cdot g^{-1}$) represents the charge-discharge specific capacitance of the electrode material, III (A) is the charging or discharging current, Δt (s) is the charging/discharging time, ΔV (V) is the voltage range during charging/discharging, and mmm (g) is the mass of the active material. Based on the specific capacitance and working voltage range of the supercapacitor, the energy and power density of the device can also be further calculated using

$$E = \frac{1}{2} C_m \Delta V^2 \times \frac{1}{3.6} \quad (2)$$

$$P = \frac{E}{\Delta t} \times 3600 \quad (3)$$

where E ($Wh \cdot kg^{-1}$) and P ($W \cdot kg^{-1}$) represent the energy density and power density of the supercapacitor, respectively, C_m is the discharge-specific capacitance of the supercapacitor, ΔV (V) is the discharge voltage range excluding the ohmic drop, and Δt (s) is the total discharge time.

RESULTS AND DISCUSSION

The phase analysis of the samples was performed using XRD. Figure 1A presents the XRD patterns of graphite, GO, and rGO. Compared to the purified natural flake graphite, the GO shows a diffraction peak at 10.8°, corresponding to its (001) crystal plane. During the hydrothermal process, GO is gradually reduced, and the characteristic peak at 10.8° disappears. Due to the removal of oxygen functional groups in GO, a small bump-like diffraction peak appears near 24.8°, corresponding to the (002) crystal plane of rGO[15]. The interlayer distance, determined via Bragg's law, is measured at 0.35 nm, surpassing the interlayer distance of graphite, which is 0.34 nm, indicating that the rGO still contains a small amount of oxygen functional groups after reduction. The broadening of the rGO peak may be attributed to the long-range disorder of the sheets and the variation in interlayer spacing caused by the presence of functional groups. Figure 1B shows the XRD spectra of Co_3S_4 and Co_3S_4/rGO-160-8 composites. The diffraction peaks near 31.4° and 50.3° correspond to the (311) and (511) crystal planes of Co_3S_4 (PDF#42-1448), confirming the successful synthesis of Co_3S_4[16]. In the XRD pattern of the Co_3S_4/rGO-160-8 composite, a broad peak is observed around 20°, corresponding to the (002) plane of rGO. This indicates a calculated interlayer distance of 0.44 nm, greater than the interlayer distance of pure rGO, measured at 0.35 nm, as illustrated in Figure 1A. The significant shift in the (002) diffraction peak observed between rGO and Co_3S_4/rGO composites can be attributed to the interaction between Co_3S_4 nanoparticles and the rGO sheets, which leads to changes in the interlayer spacing of the rGO. The introduction of Co_3S_4 onto the rGO surface can cause either an expansion or contraction of the interlayer distance, depending on the nature of the interaction. This indicates that the uniformly dispersed Co_3S_4 effectively isolates the GO sheets, preventing rGO sheet stacking. The (002) diffraction peak cannot be observed in pure Co_3S_4, further confirming the successful synthesis of the Co_3S_4/rGO-160-8 composite.

The morphological characteristics of the materials were evaluated using SEM. As shown in Figure 2A, the rGO exhibits numerous inter-stacked wrinkles, a result of the reduction of oxygen-containing functional groups during the synthesis process. In Figure 2B, Co_3S_4 is observed to form micro-rods composed of dense nanoparticles that are agglomerated together. Figure 2C and D demonstrates that the micro-rod structure shows good dispersion on the surface of rGO after composite formation via hydrothermal synthesis. Cobalt ions bind to negatively charged oxygen atoms, adsorbing and growing on the GO nanosheets. During the sulfide process, S^{2-} from sodium sulfide undergoes ion exchange to form Co_3S_4 while GO is reduced to rGO.

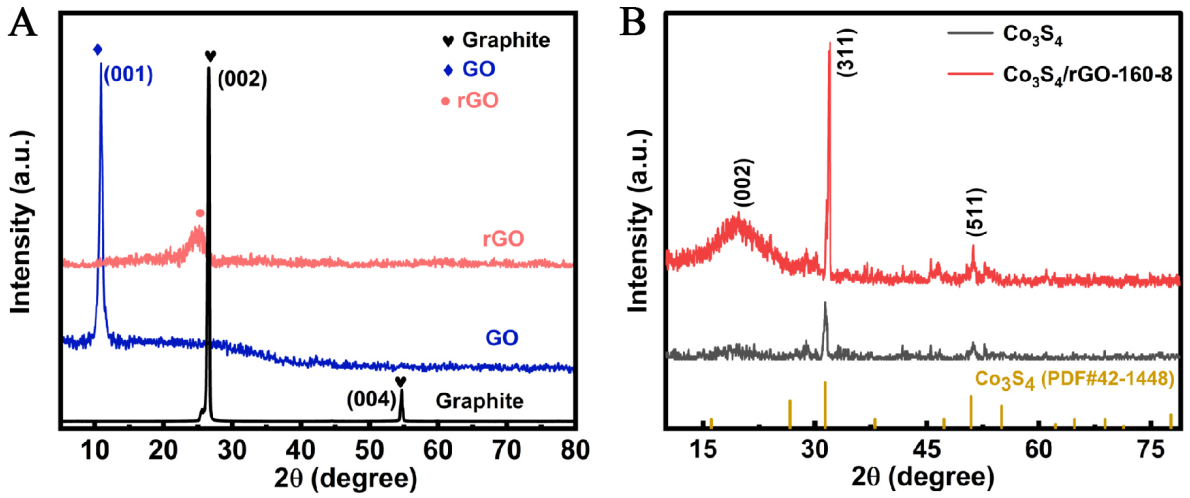

Figure 1. (A) shows the XRD patterns of graphite, GO, and rGO; (B) displays the XRD patterns of Co_3S_4 and Co_3S_4/rGO-160-8. rGO:reduced graphene oxide; GO: graphene oxide; XRD: X-ray diffraction.

This indicates that the graphene sheets serve as a conductive network framework, facilitating the dispersion of the rod-like material, preventing agglomeration, shortening the ionic transport path, and improving the rate performance of the active material, thus providing a larger electrochemical active area[17]. Cobalt ions can bind to the functional groups of oxidized graphene, thereby enhancing interfacial contact and facilitating improved interactions between the electrode and surrounding electrolyte ions.

TEM further explores the microstructure and crystalline structure of Co_3S_4/rGO-160-8. Figure 2E clearly shows Co_3S_4 rods completely covered by rGO, with a rod length of approximately 300 nm. The introduction of graphene provides a growth substrate for the Co_3S_4 rods, and the combination of both offers a conductive network and rapid ionic diffusion pathways for redox reactions. Figure 2F is the high-resolution TEM (HRTEM) image of the Co_3S_4/rGO-160-8 electrode, displaying lattice fringes of 0.24 nm and 0.18 nm, corresponding to the (311) and (511) crystal planes of Co_3S_4, further confirming the formation of Co_3S_4 in rGO[18]. Figure 2G presents high-angle annular dark-field scanning TEM (HAADF-STEM) images alongside energy dispersive spectroscopy (EDS) elemental mapping of the Co_3S_4/rGO-160-8 composite. In the carbon distribution map, except for signals from the carbon support film, the remaining carbon signals are distributed over the graphene sheets. The oxygen elements are mainly found on the graphene sheets, primarily as residual oxygen functional groups. Meanwhile, cobalt and sulfur elements are predominantly distributed on the Co_3S_4 rods, further validating the successful preparation of the Co_3S_4/rGO-160-8 composite.

XPS was employed to investigate the elemental composition and chemical states of the Co_3S_4/rGO-160-8 material. The full-scan XPS spectrum of Co_3S_4/rGO-160-8 [Supplementary Figure 1] displays characteristic peaks at 162.2, 284.8, 532.1, and 778.7 eV, corresponding to S 2p, C 1s, O 1s, and Co 2p, respectively, confirming the presence of sulfur, carbon, oxygen, and cobalt in the material. Figure 3A presents the XPS spectrum of the Co 2p region, where the $2p_{3/2}$ and $2p_{1/2}$ peaks for Co in the + 3 oxidation state appear at 778.8 and 794.1 eV, while those for Co in the + 2 oxidation state are found at 781.2 and 797.3 eV. This indicates the coexistence of Co^{3+} and Co^{2+} in the material[19]. Additionally, the binding energies at 786.7 and 803.1 eV correspond to satellite peaks of Co 2p. Figure 3B illustrates the C 1s spectrum, where the peak for C-C/C = C bonds is observed at 284.8 eV, while peaks for C-O/C-S and C = O bonds are located at 286 and 289.3 eV, respectively, indicating the successful reduction of GO during the material preparation. The high-

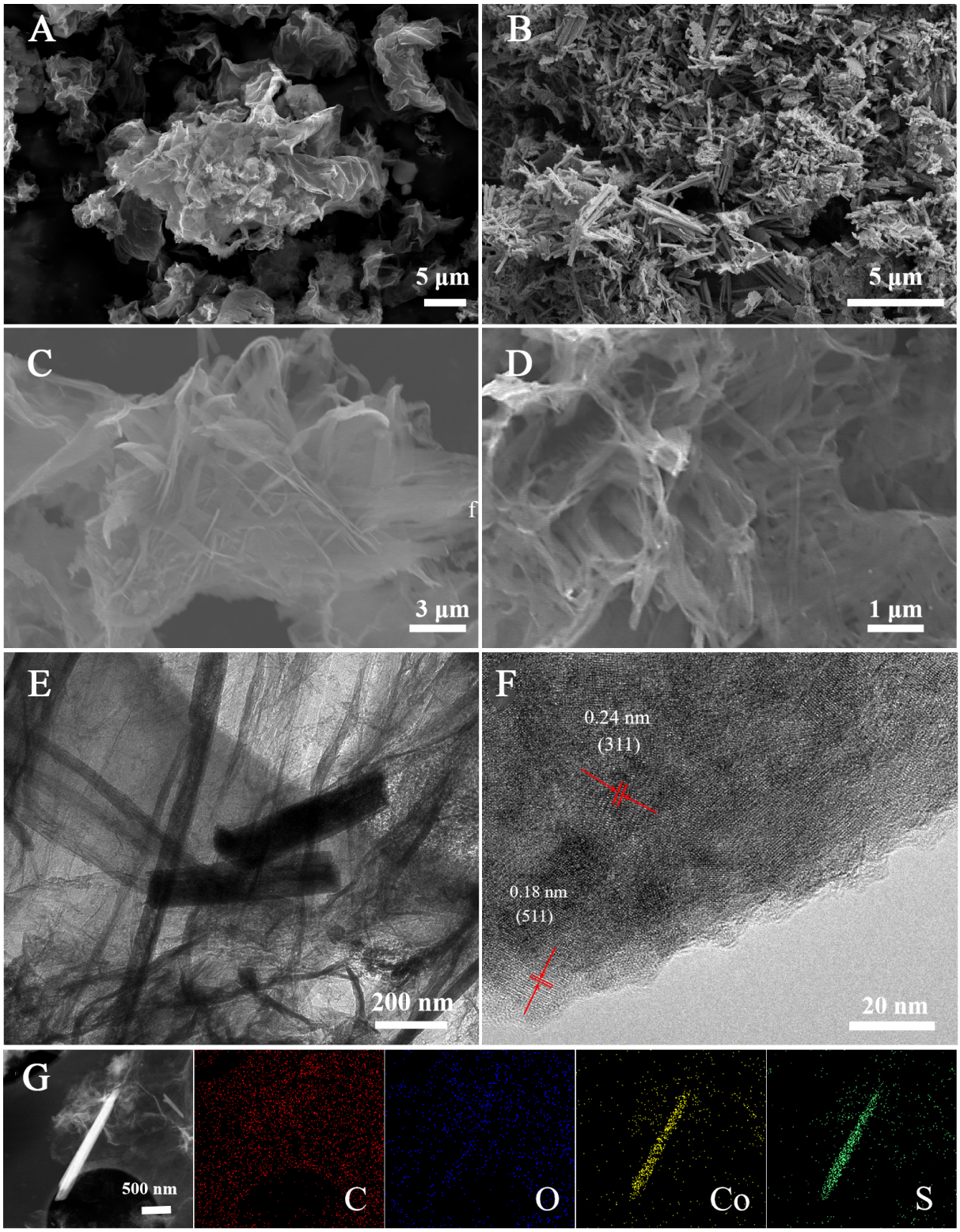

Figure 2. The (A-D) SEM image; (E, F) HRTEM image; (G) HAADF-STEM image and EDS elemental mapping of the Co3S4/rGO-160-8 electrode. SEM: scanning electron microscopy; HRTEM: high-resolution transmission electron microscopy; HAADF-STEM: high-angle annular dark-field scanning transmission electron microscopy; EDS: energy dispersive spectroscopy.

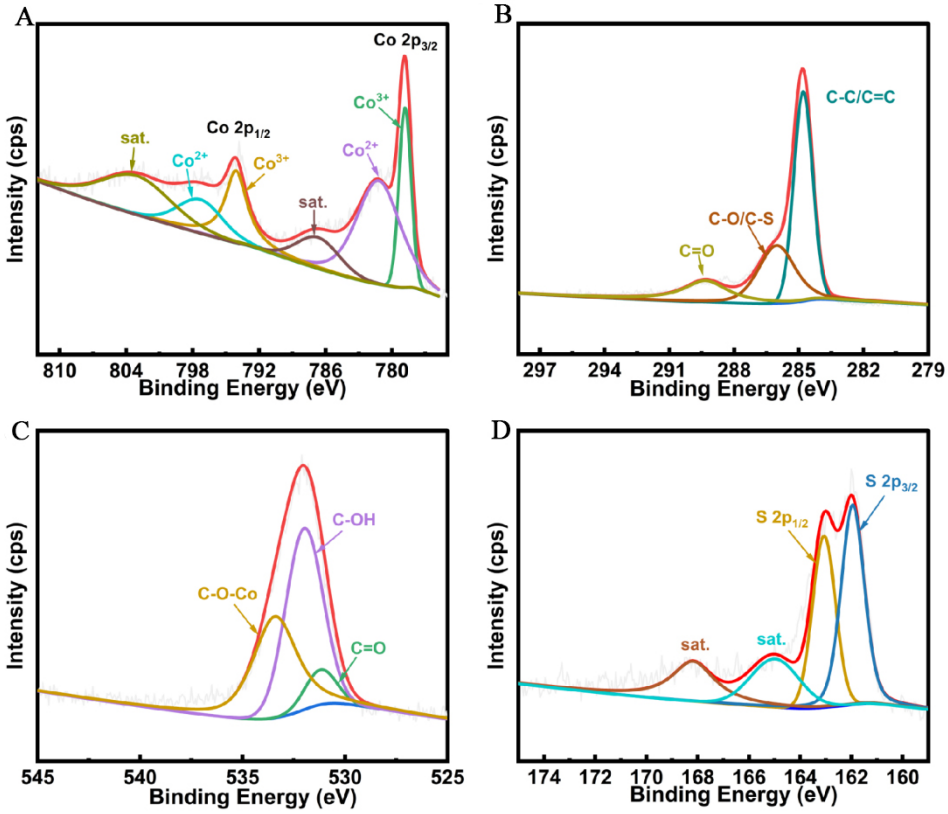

Figure 3. High-resolution XPS survey spectra of (A) Co 2p; (B) C 1s; (C) O 1s; (D) S 2p spectra of Co_3S_4/rGO-160-8 and rGO materials. XPS: X-ray photoelectron spectroscopy; rGO:reduced graphene oxide.

resolution O 1s spectrum [Figure 3C] can be divided into three components: C = O (531.2 eV), C-OH (532 eV), and C-O-Co (533.4 eV), with C = O and C-OH arising from oxygen-containing functional groups on the graphene surface. In Figure 3D, the fitted spectrum of the S 2p region shows a characteristic peak at 161.9 eV corresponding to $2p_{3/2}$ of S^{2-} , indicating that the synthesized material consists of metal-sulfur bonds, while the peak at 163.1 eV corresponds to $2p_{1/2}$ of S^{2-}, indicating sulfur bonded to carbon, thus confirming the presence of S^{2-}[20]. This suggests that sulfur is incorporated within the graphene nanosheets, and during the formation of Co_3S_4, $Na_2S{\cdot}9H_2O$ provides sulfur atoms that may simultaneously incorporate into the rGO. Furthermore, the fitted peaks at 164.9 and 168.2 eV correspond to satellite peaks of S 2p. Consequently, the XPS results further demonstrate the successful synthesis of the Co_3S_4/rGO-160-8 composite material.

Figure 4A depicts the Raman spectra of Co_3S_4/rGO-160-8 and rGO. The peak at 1350 cm^{-1} corresponds to the D band, which is linked to sp^3 defects in carbon-based materials, whereas the peak at 1590 cm^{-1} is attributed to the G band, reflecting the intensity of sp^2 hybridization. The I_D/I_G ratio, which is commonly used to measure the defect level in graphene, is 1.17 for Co_3S_4/rGO-160-8, significantly higher than the corresponding value for GO (0.96), indicating the successful reduction of rGO in Co_3S_4/rGO-160-8[21]. The introduction of Co_3S_4 during the composite process leads to more defects on the graphene sheets, providing additional charge storage space for the composite material. Furthermore, an additional peak at 667 cm^{-1} in the Raman spectrum of Co_3S_4/rGO-160-8 is attributed to the A1g vibration mode of Co_3S_4, further confirming its successful anchoring on the graphene sheets. Figure 4B shows the TGA curve of the Co_3S_4/rGO-160-8 sample, revealing three weight loss stages throughout the process. The first weight loss from

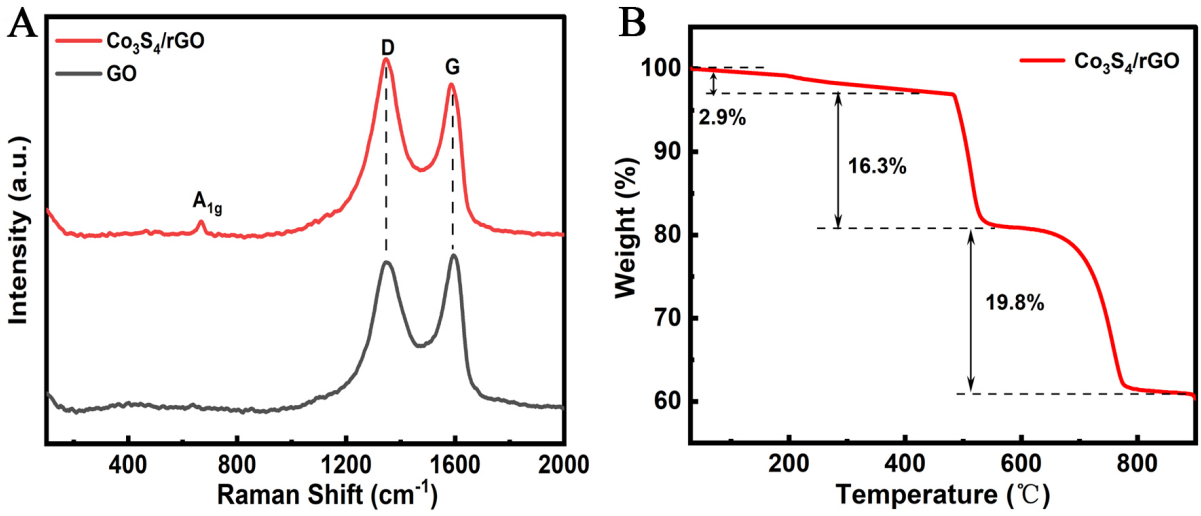

Figure 4. (A) Raman spectra of Co_3S_4/rGO-160-8 and GO; (B) TGA curve of Co_3S_4/rGO-160-8. rGO:reduced graphene oxide; GO: graphene oxide; TGA: thermogravimetric analysis.

room temperature to 400 °C, approximately 2.9%, is attributed to the evaporation of moisture retained in the sample. The weight loss from 400 to 550 °C, approximately 16.3%, is due to the oxidation of rGO to CO_2 in air. The third stage (500 to 800 °C) corresponds to the oxidation of Co_3S_4 to Co_3O_4, presenting a weight loss of 19.8%[22]. Thus, the weight compositions of Co_3S_4 and graphene in the Co_3S_4/rGO-160-8 composite material can be determined as 83.2% and 16.8%, respectively.

Structural characterization confirms that Co_3S_4/rGO-160-8 is the optimal electrode material. To validate this finding, electrochemical tests were conducted using a three-electrode system in a 6.0 mol·L^{-1} KOH electrolyte. Figure 5A presents the CV curves for various samples at a scan rate of 10 mV·s^{-1} within the voltage range of 0 to 0.5 V. All samples display clear oxidation and reduction peaks in the CV curves, indicative of characteristic pseudocapacitive behavior. The Faradaic reactions occurring in alkaline electrolyte are given as follows[23]:

$$Co_3S_4 + OH^- \leftrightarrow Co_3S_4OH + e^- \quad (4)$$

$$Co_3S_4OH + OH^- \leftrightarrow Co_3S_4O + H_2O + e^- \quad (5)$$

Additionally, with increasing scan rates, the peak potentials of both anodic and cathodic currents exhibit shifts toward higher and lower values, respectively, likely attributed to polarization effects. The peak current also increases correspondingly, attributable to overpotentials in ion transport at the electrode-electrolyte interface[24]. The gradual decrease in capacitance may be linked to the charge resistance of the electrode material at higher scan rates, along with the diffusion of ions lagging behind electron mobility. Notably, all curves display similar shapes, confirming the reversibility of redox reactions at the Co_3S_4/rGO-160-8 electrode. As the scan rate increases, the rapid transfer of electrons and ions at the electrode surface leads to an increase in the integrated area of the CV curve, indicating efficient ion and electron transport at high scan rates. The rGO nanosheets can easily wrap around the surface of Co_3S_4 tubes, serving as a conductive support and providing a larger surface area. Figure 5B illustrates the correlation between peak current and

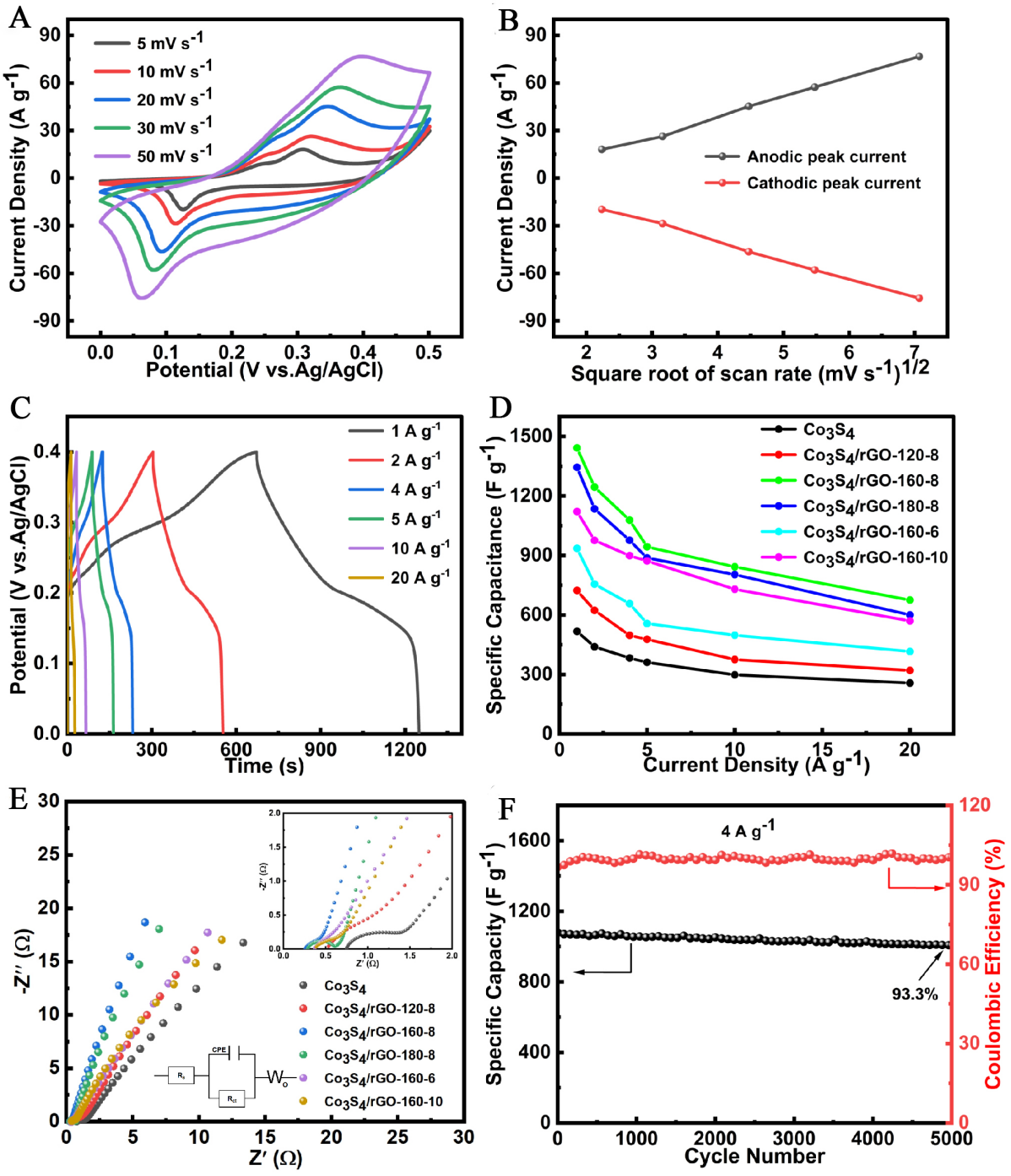

Figure 5. (A) CV curves at different scan rates for Co_3S_4/rGO-160-8; (B) the relationship between peak current and the square root of scan rate; (C) GCD curves for Co_3S_4/rGO-160-8 at different current densities; (D) Rate performance of different electrode materials; (E) Nyquist plots for different electrode materials; (F) Cycling performance of Co_3S_4/rGO-160-8 at 4 $A \cdot g^{-1}$.CV: cyclic voltammetry; GCD: displays the galvanostatic charge-discharge; rGO:reduced graphene oxide.

the square root of the scan rate for the Co_3S_4/rGO-160-8 electrode, showing a strong linear trend that indicates good reversibility of the material. This linear relationship further suggests that the redox reactions at the electrode surface are diffusion-controlled by the electrolyte.

Figure 5C presents the GCD curves of Co_3S_4/rGO-160-8 at different current densities, revealing charge-discharge platforms that indicate the existence of redox reactions during testing, in accordance with the earlier CV analysis. The excellent symmetry of all GCD curves further substantiates the reversibility of the electrode material. Based on discharge times, the specific capacitances for Co_3S_4/rGO-160-8 at current densities of 1, 2, 4, 5, 10, and 20 $A \cdot g^{-1}$ are approximately 1442.5, 1244.5, 1078.0, 943.8, 842.5, and 675.0 $F \cdot g^{-1}$, respectively. Specific capacitance calculations for Co_3S_4 and Co_3S_4/rGO-160-8 under different conditions are shown in Figure 5D. At the same current density, the Co_3S_4/rGO-160-8 electrode exhibits higher capacitance than other materials. It is noteworthy that the specific capacitance values for all electrodes exhibit a decreasing trend with increasing scan rates, attributed to ion diffusion rates. At higher scan rates, fewer ions penetrate the electrode material for reactions, resulting in lower specific capacitance. Even at an elevated current density of 20 $A \cdot g^{-1}$, the Co_3S_4/rGO-160-8 electrode maintains a capacitance of 675.0 $F \cdot g^{-1}$, significantly surpassing other materials, indicating effective ion and charge transport under rapid redox conditions. The charge storage was calculated from the integrated area of the CV curves, yielding a value of 468.06 mAh/g at a scan rate of 10 mV/s, which suggests efficient charge storage and a high rate capability[25].

The EIS data presented in this study provide valuable insight into the conductivity and charge transfer characteristics of the electrode materials [Figure 5E]. The Rs, Rct, and Warburg impedance (Zw) values derived from the EIS spectra reflect the internal resistance, the resistance for charge transfer at the electrode/electrolyte interface, and the diffusion of ions within the material, respectively. The observed values for Co_3S_4 and Co_3S_4/rGO composites show significant differences in charge transport properties, highlighting the influence of material structure and composition on electrochemical performance. For example, the Co_3S_4/rGO-160-8 electrode exhibits the lowest Rs and Rct values (0.26 Ω and 0.41 Ω, respectively), suggesting superior electron conductivity and efficient charge transfer at the electrode interface. The improvement in conductivity for the Co_3S_4/rGO composites compared to pure Co_3S_4 can be attributed to the inclusion of rGO. Graphene, known for its excellent electronic conductivity, forms a conductive network that facilitates electron transport, reducing the Rs of the composite material. This effect is especially pronounced in the Co_3S_4/rGO-160-8 composite, where the optimized synthesis conditions (160 °C for 8 h) enable the formation of a more uniform composite structure, thereby enhancing electron conductivity[26]. The Rct is another critical factor influencing the electrochemical performance of the electrode material. A lower Rct indicates more efficient charge transfer at the electrode/electrolyte interface. The Co_3S_4/rGO-160-8 composite, with the lowest Rct, suggests that the inclusion of rGO not only improves the electron conductivity but also enhances the interaction between the electrode material and the electrolyte, facilitating faster electron transfer. This is in line with the observed higher slope in the low-frequency region of the EIS spectrum for the Co_3S_4/rGO-160-8 electrode. In supercapacitors, a larger slope in the low-frequency region is indicative of ideal capacitive behavior, where rapid and reversible ion adsorption/desorption occurs at the electrode/electrolyte interface. The faster ion desorption/adsorption implies more efficient ion transport within the material, leading to higher capacitance. The Zw observed in the EIS data is linked to the ion diffusion process within the material, particularly at lower frequencies. The slope of the EIS curve at these lower frequencies provides information on the rate of ion diffusion and the ability of the material to accommodate ion movement within its structure. In the case of the Co_3S_4/rGO-160-8 electrode, the higher slope at low frequencies suggests faster ion diffusion, which can be attributed to the improved microstructure of the composite. The combination of rGO's high surface area and the rod-like Co_3S_4 nanoparticles creates an interconnected network that provides more accessible pathways for ion transport[27]. This, in turn, minimizes polarization effects during charge/discharge cycles and leads to enhanced electrochemical capacitance performance. In contrast, the Co_3S_4 electrode, which lacks the conductive rGO component, exhibits higher Rs and Rct values, reflecting slower electron transfer and ion diffusion. This limitation is primarily due to the intrinsic poor conductivity of Co_3S_4 and the lack of a conductive network, which hampers the efficient movement of charge carriers and ions. Overall, the EIS

results suggest that the Co_3S_4/rGO composites, particularly Co_3S_4/rGO-160-8, benefit from the synergistic effects of the Co_3S_4 nanoparticles and rGO, resulting in enhanced electron conductivity, efficient charge transfer, and faster ion diffusion. These factors contribute to the improved electrochemical performance of the composite material, including higher capacitance, better rate performance, and enhanced cycling stability. The findings highlight the critical role of microstructural design in optimizing the electrochemical properties of supercapacitor electrodes and demonstrate the potential of rGO-based composites for high-performance energy storage applications.

Cycling performance is a critical parameter for evaluating the practical applicability of electrode materials. GCD cycling tests conducted at 4 $A \cdot g^{-1}$ reveal the variations in specific capacitance and Coulombic efficiency for the Co_3S_4/rGO-160-8 electrode over 5000 cycles, as shown in Figure 5F, where the capacitance only decreased by 6.7%. Throughout the cycling period, the Coulombic efficiency approached nearly 100%, confirming the high reversibility of the Faradaic reactions during charge and discharge. The composite material, based on graphene, possesses both chemical and mechanical stability, effectively buffering volume change stresses and reducing the likelihood of structural damage[28]. Thus, the resultant Co_3S_4/rGO-160-8 composite exhibits excellent cycling stability.

To evaluate the application of the Co_3S_4/rGO-160-8 electrode material, an asymmetric supercapacitor was fabricated utilizing Co_3S_4/rGO-160-8 as the positive electrode and AC as the negative electrode, designated as Co_3S_4/rGO-160-8//AC. The active mass ratio of the positive electrode to the negative electrode was determined to be 1:3.1. The electrochemical performance of the device was tested in a 6 $mol \cdot L^{-1}$ KOH electrolyte, with results shown in Figure 6. Figure 6A displays the CV curves of AC and Co_3S_4/rGO-160-8 electrode materials at a scan rate of 10 $mV \cdot s^{-1}$. The Co_3S_4/rGO-160-8 electrode exhibited pseudocapacitive characteristics within a voltage range of 0-0.5 V, while the AC showed electric double-layer capacitance features within the voltage range of -1.0 to 0 V. By combining these two electrodes, the constructed asymmetric supercapacitor not only possesses pseudocapacitive properties but also features double-layer capacitance. This configuration enables a higher operational voltage by integrating the voltage ranges of both electrodes, resulting in an estimated operational voltage range of 0-1.5 V for the Co_3S_4/rGO-160-8//AC device.

Figure 6B presents the CV curves of the Co_3S_4/rGO-160-8//AC supercapacitor within a voltage window of 0-1.5 V at various scan rates. The curves exhibit a broad redox peak, which is attributed to the distinct energy storage mechanisms of the two electrodes. The integral area of the CV curve increases with the rising scan rate, and the current values of the redox peaks also increase, while the basic shape of the curve remains stable. This trend indicates that the device exhibits excellent rapid charge-discharge capabilities and good rate performance[29]. Figure 6C displays the galvanostatic charge-discharge (GCD) curves for the Co_3S_4/rGO-160-8//AC supercapacitor within the voltage range of 0-1.5 V. The curves display good symmetry, suggesting that the redox reactions of Co_3S_4/rGO-160-8//AC are reversible. The specific capacitance of the device was determined using Equation (1), where mmm denotes the total active mass of Co_3S_4/rGO-160-8 and AC. The EIS results reveal interesting trends when comparing the impedance of the supercapacitor device before and after cycling [Supplementary Figure 1]. Notably, after 5000 cycles, the overall impedance decreases, with a reduction in Rs and an increase in the slope of the low-frequency region. Typically, one would expect an increase in resistance due to side reactions or structural degradation, but the observed decrease in Rs suggests a beneficial evolution of the material during cycling. This could be due to structural reorganization that improves the contact between the active material and the conductive network, enhancing electrical conductivity. The increase in the slope of the low-frequency region suggests faster ion diffusion and better charge transfer at the electrode/electrolyte interface, indicating reduced polarization

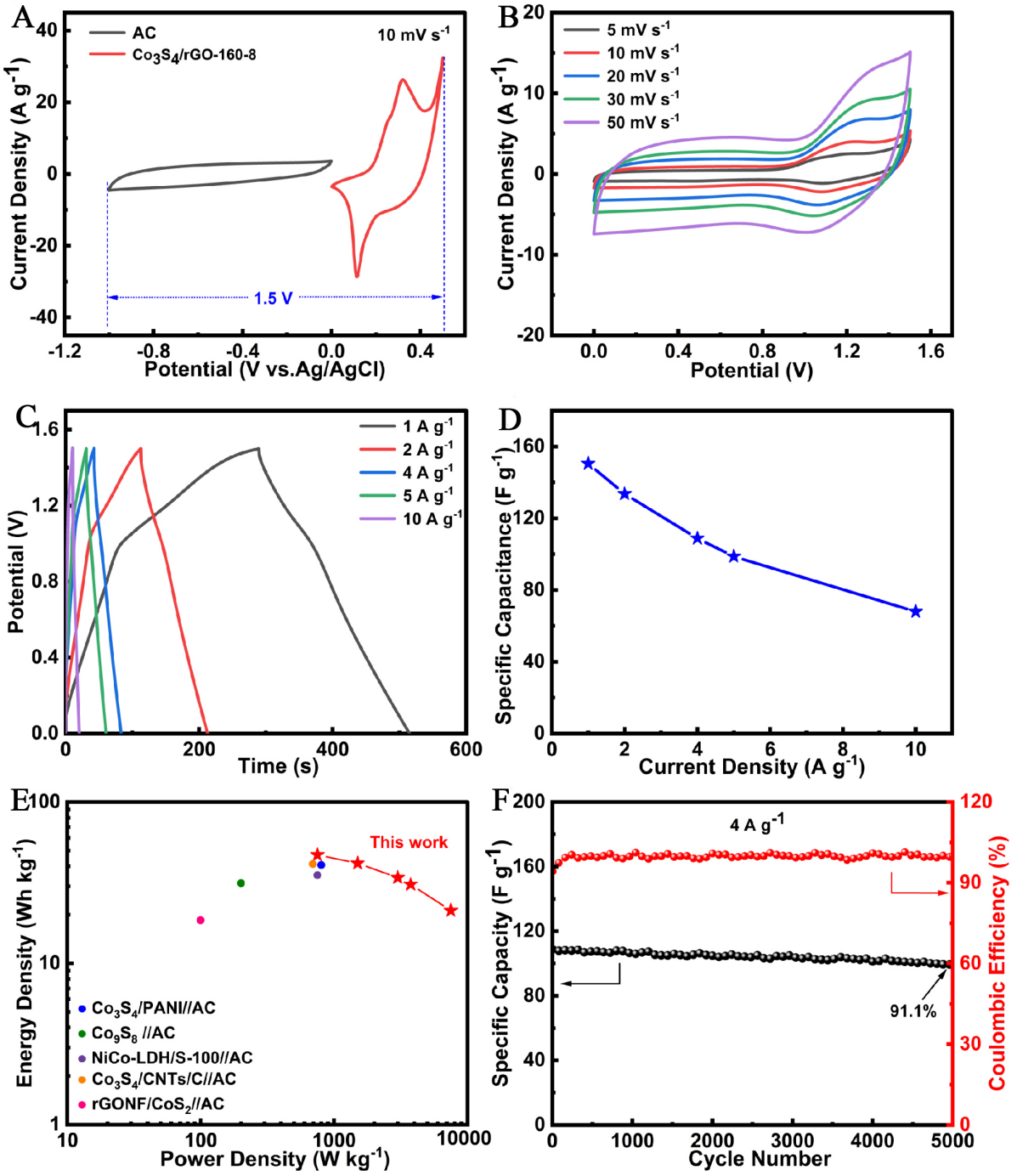

Figure 6. (A) CV curves of AC and Co_3S_4/rGO-160-8 at 10 mV·s^{-1}; (B) CV curves of Co_3S_4/rGO-160-8//AC at different scan rates; (C) GCD curves of Co_3S_4/rGO-160-8//AC at different current densities; (D) Rate performance; (E) Ragone plot of Co_3S_4/rGO-160-8//AC; (F) Cycling stability and Coulombic efficiency at a current density of 4 A·g^{-1}. CV: cyclic voltammetry; AC: activated carbon; rGO:reduced graphene oxide; GCD: displays the galvanostatic charge-discharge.

effects. The results are shown in Figure 6D. At a current density of 1·A g^{-1}, the device exhibits a specific capacitance value of 150.5 F·g^{-1}, demonstrating good energy storage performance[30]. As the current density rises to 10 A·g^{-1}, the capacitance declines to 68.0 F·g^{-1}. This decrease in capacitance with increasing current

density is attributed to the limited time available for the positive and negative electrodes to adequately respond, leading to a decrease in the active materials participating in the reaction.

The key performance indicators for evaluating energy storage devices include energy and power densities. Utilizing the results obtained from the GCD tests, the energy and power densities of the Co_3S_4/rGO-160-8//AC device were determined using Equations (2) and (3), where mmm represents the total mass of both the positive and negative electrodes. The results are plotted in Figure 6E, showing that at a power density of 749.8 $W{\cdot}kg^{-1}$, the Co_3S_4/rGO-160-8//AC device achieves an energy density of 47.0 $Wh{\cdot}kg^{-1}$. Even when the power density is increased to 7500.0 $W{\cdot}kg^{-1}$, the energy density remains at 21.3 $Wh{\cdot}kg^{-1}$. Compared to previously reported devices assembled with transition metal sulfides, this device exhibits superior energy and power densities. For example, Co_3S_4/PANI//AC achieves 40.75 $Wh{\cdot}kg^{-1}$ at 800 $W{\cdot}kg^{-1}$[31], Co_9S_8//AC delivers 31.4 Wh kg^{-1} at 200 W kg^{-1}[32], NiCo-LDH/S-100//AC reaches 35.21 Wh kg^{-1} at 749.98 $W{\cdot}kg^{-1}$[33], Co_3S_4/CNTs/C//AC provides 41.3 $Wh{\cdot}kg^{-1}$ at 691.9 $W{\cdot}kg^{-1}$[34], and rGO-NF/CoS_2//AC shows 18.5 $Wh{\cdot}kg^{-1}$ at 99.8 $W{\cdot}kg^{-1}$[35].

Figure 6F presents the cycling stability test of the Co_3S_4/rGO-160-8//AC device. As shown, after 5000 GCD tests at 4 $A{\cdot}g^{-1}$, the device retains 91.1% of its capacity, indicating excellent cycling stability. Additionally, the Coulombic efficiency during the cycling tests approaches 100%, demonstrating good charge-discharge reversibility. These results suggest that rGO sheets, as a two-dimensional carbon allotrope, not only facilitate the formation of electric double layers but also serve as a high-surface support, enabling strong anchoring of Co_3S_4 nanotubes without agglomeration. The direct deposition of Co_3S_4 onto the surface of rGO not only enhances the specific capacitance of the rGO but also promotes charge transfer while effectively preventing the aggregation and restacking of rGO, increasing the active surface area available for charge storage. These findings indicate the significant application potential of this material in energy storage devices.

CONCLUSIONS

In this work, Co_3S_4/rGO composites were prepared by a two-step hydrothermal synthesis procedure, exploring the effects of sulfurization temperature and time on their electrochemical performance. The results indicated that the Co_3S_4/rGO-160-8 electrode material, synthesized at a sulfurization temperature of 160 °C for eight hours, exhibited optimal electrochemical properties. Three-electrode tests were conducted on the samples, and an asymmetric supercapacitor was assembled using Co_3S_4/rGO-160-8 and AC electrodes for further electrochemical performance evaluation. It was concluded that the rGO sheets serve as a substrate to form a conductive network, enhancing the conductivity of the composite materials. Electrochemical testing showed that the Co_3S_4/rGO-160-8 material displayed the highest capacitance at the specified sulfurization conditions, achieving a mass-specific capacitance of 1442.5 $F{\cdot}g^{-1}$ at 1 $A{\cdot}g^{-1}$. Additionally, after 5000 cycles of GCD at 4 A g^{-1}, the specific capacitance retained 93.3% of its initial value, indicating a significant enhancement in performance compared to bare Co_3S_4 electrode materials. The asymmetric supercapacitor assembled with Co_3S_4/rGO-160-8 and AC achieved an energy density of 47.0 $Wh{\cdot}kg^{-1}$ at a power density of 749.8 $W{\cdot}kg^{-1}$. Notably, it maintained a specific capacitance retention of 91.1% after 5000 cycles at 4 $A{\cdot}g^{-1}$, showcasing outstanding cycling stability. This high-performance electrode material presents a viable solution for utilizing natural graphite in energy storage devices.

DECLARATIONS

Authors' contributions

Made substantial contributions to conception and design of the study and performed data analysis and interpretation: Wang, G. L.; Zhao, J.; Wen, Q.

Performed data acquisition and provided administrative, technical, and material support: Zhu, M. X.; Liu, H; Han, X. L.; Zhang, K. M.; Li, C. Y.; Sun, H. R.

Availability of data and materials

The rata data supporting the findings of this study are available within this Article and its Supplementary Information. Further data are available from the corresponding authors upon request.

Financial support and sponsorship

This work was supported by the Heilongjiang Province key research and development plan (2023ZXJ05A01) and the Key Program of Jixi Natural Science Foundation (JKZZ2023R01; JKZT2022R03; JKZZ2022R01).

Conflicts of interest

Mingxing Zhu, Xinlei Han, Kaiming Zhang, Chunyu Li, and Hongru Sun are affiliated with Heilongjiang Longxing International Resources Development Group Co., Ltd. Huan Liu, Qing Wen, Jing Zhao, and Guiling Wang are affiliated with Heilongjiang Hachuan Carbon Materials Technology Co., LTD. Jing Zhao is Guest Editor Assistant of the Special Issue "Microstructure Modulation and Optimization of Aqueous Batteries" but was not involved in any steps of editorial processing, notably including reviewer selection, manuscript handling or decision-making.

Ethical approval and consent to participate

Not applicable.

Consent for publication

Not applicable.

REFERENCES

1. Wang, X.; Su, C.; Xue, Z.; Xie, X. Sustainable development goals perspective of natural resources: does it paves the way for renewable sources of energy? *Resour. Policy.* **2023**, *86*, 104075. DOI
2. Tian, H.; Wang, K.; Cui, X.; Chen, Z.; Zhao, E.; Saeedi, S. RETRACTED: Multi-objective planning of microgrid based on renewable energy sources and energy storage system. *J. Energy. Storage.* **2023**, *68*, 107803. DOI
3. Sahoo, S.; Milton, A.; Sood, A.; et al. Microwave-assisted synthesis of perovskite hydroxide-derived Co_3O_4/SnO_2/reduced graphene oxide nanocomposites for advanced hybrid supercapacitor devices. *J. Energy. Storage.* **2024**, *99*, 113321. DOI
4. Sharma, R.; Kumar, H.; Kumar, G.; et al. Progress and challenges in electrochemical energy storage devices: Fabrication, electrode material, and economic aspects. *Chem. Eng. J.* **2023**, *468*, 143706. DOI
5. Zhang, S.; Li, Y.; Du, E.; et al. A review and outlook on cloud energy storage: An aggregated and shared utilizing method of energy storage system. *Renew. Sust. Energy. Rev.* **2023**, *185*, 113606. DOI
6. Zhu, F.; Ge, J.; Gao, Y.; et al. Molten salt electro-preparation of graphitic carbons. *Exploration. (Beijing).* **2023**, *3*, 20210186. DOI PubMed PMC
7. Yang, W.; Wang, J.; Jian, J. Metal organic framework-based materials for metal-ion batteries. *Energy. Storage. Mater.* **2024**, *66*, 103249. DOI
8. Kumar, R.; Sahoo, S.; Pandey, R.; Joanni, E.; Yadav, R. M. Electromagnetic irradiation-assisted synthesis, exfoliation and modification of graphene-based materials for energy storage and sensing applications. *Mater. Sci. Eng:. R:. Rep.* **2024**, *161*, 100860. DOI
9. Wang, T.; Wang, Y.; Lei, J.; Chen, K. J.; Wang, H. Electrochemically induced surface reconstruction of Ni-Co oxide nanosheet arrays for hybrid supercapacitors. *Exploration. (Beijing).* **2021**, *1*, 20210178. DOI PubMed PMC
10. Naeem, S.; Patil, A. V.; Shaikh, A. V.; et al. A review of cobalt-based metal hydroxide electrode for applications in supercapacitors. *Adv. Mater. Sci. Eng.* **2023**, *2023*, 1-15. DOI
11. Mishra, S.; Maurya, P. K.; Mishra, A. K. 2H–MoS_2 nanoflowers based high energy density solid state supercapacitor. *Mater. Chem.*

Phys. **2020**, *255*, 123551. DOI
12. Zhou, Y.; Li, N.; Sun, L.; et al. Multi-layer-stacked Co_9S_8 micro/nanostructure directly anchoring on carbon cloth as a flexible electrode in supercapacitors. *Nanoscale* **2019**, *11*, 7457-64. DOI
13. Ren, H.; Xia, X.; Sun, Y.; et al. Electrolyte engineering for the mass exfoliation of graphene oxide across wide oxidation degrees. *J. Mater. Chem. A.* **2024**, *12*, 23416-24. DOI
14. Yang, J.; Duan, X.; Guo, W.; Li, D.; Zhang, H.; Zheng, W. Electrochemical performances investigation of NiS/rGO composite as electrode material for supercapacitors. *Nano. Energy.* **2014**, *5*, 74-81. DOI
15. Jiang, H.; Dai, Y.; Hu, Y.; Chen, W.; Li, C. Nanostructured ternary nanocomposite of rGO/CNTs/MnO_2 for high-rate supercapacitors. *ACS. Sustainable. Chem. Eng.* **2014**, *2*, 70-4. DOI
16. Li, H.; Yang, H.; Sun, Z.; Shi, Y.; Cheng, H.; Li, F. A highly reversible Co_3S_4 microsphere cathode material for aluminum-ion batteries. *Nano. Energy.* **2019**, *56*, 100-8. DOI
17. Sahu, N.; Behera, J. N. MOF-derived Co_3S_4 nanoparticles embedded in nitrogen-doped carbon for electrochemical oxygen production. *ACS. Appl. Nano. Mater.* **2023**, *6*, 7686-93. DOI
18. Nandhini, S.; Muralidharan, G. Co_3S_4-CoS/rGO hybrid nanostructure: promising material for high-performance and high-rate capacity supercapacitor. *J. Solid. State. Electrochem.* **2021**, *25*, 465-77. DOI
19. Wang, Q.; Jiao, L.; Du, H.; Si, Y.; Wang, Y.; Yuan, H. Co_3S_4 hollow nanospheres grown on graphene as advanced electrode materials for supercapacitors. *J. Mater. Chem.* **2012**, *22*, 21387. DOI
20. Zhang, Q.; Xu, C.; Lu, B. Super-long life supercapacitors based on the construction of Ni foam/graphene/Co_3S_4 composite film hybrid electrodes. *Electrochim. Acta.* **2014**, *132*, 180-5. DOI
21. He, G.; Bai, Y.; Huangfu, H.; et al. Enhanced electrochemical energy storage of rGO@Co_xS_y through nanostructural modulation. *J. Mater. Sci:. Mater. Electron.* **2021**, *32*, 13639-55. DOI
22. Wu, Y. Q.; Yang, H. X.; Yang, Y.; et al. SnS_2 /Co_3S_4 hollow nanocubes anchored on S-doped graphene for ultrafast and stable Na-ion storage. *Small* **2019**, *15*, e1903873. DOI
23. Yang, Y. J.; Li, W.; Chen, S.; et al. Assembly of Co_3S_4-encapsulated reduced graphene oxide nanosheets on Ni foam for binder-free supercapacitor electrode with boosted cycling stability. *Ionics* **2023**, *29*, 2899-909. DOI
24. Wei, G.; Yan, L.; Huang, H.; et al. The hetero-structured nanoarray construction of Co_3O_4 nanowires anchored on nanoflakes as a high-performance electrode for supercapacitors. *Appl. Surf. Sci.* **2021**, *538*, 147932. DOI
25. Ma, Q.; Cui, F.; Zhang, J.; Qi, X.; Cui, T. Surface engineering of Co_3O_4 nanoribbons forming abundant oxygen-vacancy for advanced supercapacitor. *Appl. Surf. Sci.* **2022**, *578*, 152001. DOI
26. Zhao, J.; Zhang, Y.; Wang, Y.; Li, H.; Peng, Y. The application of nanostructured transition metal sulfides as anodes for lithium ion batteries. *J. Energy. Chem.* **2018**, *27*, 1536-54. DOI
27. Nandhini, S.; Muralidharan, G. The binder-free mesoporous $CoNi_2S_4$ electrode for high-performance symmetric and asymmetric supercapacitor devices. *J. Mater. Sci.* **2022**, *57*, 5933-53. DOI
28. Ma, Y.; Xie, X.; Yang, W.; et al. Recent advances in transition metal oxides with different dimensions as electrodes for high-performance supercapacitors. *Adv. Compos. Hybrid. Mater.* **2021**, *4*, 906-24. DOI
29. Ma, M.; Yao, Y.; Wu, Y.; Yu, Y. Progress and prospects of transition metal sulfides for sodium storage. *Adv. Fiber. Mater.* **2020**, *2*, 314-37. DOI
30. Zhou, J.; Chen, J.; Peng, Y.; Zheng, Y.; Zeb, A.; Lin, X. Metal-organic framework-derived transition metal sulfides and their composites for alkali-ion batteries: a review. *Coord. Chem. Rev.* **2022**, *472*, 214781. DOI
31. Xu, M.; Guo, H.; Zhang, T.; Zhang, J.; Wang, X.; Yang, W. High-performance zeolitic imidazolate frameworks derived three-dimensional Co_3S_4/polyaniline nanocomposite for supercapacitors. *J. Energy. Storage.* **2021**, *35*, 102303. DOI
32. Rakhi, R. B.; Alhebshi, N. A.; Anjum, D. H.; Alshareef, H. N. Nanostructured cobalt sulfide-on-fiber with tunable morphology as electrodes for asymmetric hybrid supercapacitors. *J. Mater. Chem. A.* **2014**, *2*, 16190-8. DOI
33. Yang, C.; Song, F.; Chen, Q. Composites of NiCo layered double hydroxide nanosheets and Co_3S_4 nanoparticles for asymmetric supercapacitors. *ACS. Appl. Nano. Mater.* **2023**, *6*, 10804-16. DOI
34. Qiao, Y.; Wang, F.; Li, N.; Gao, W.; Jiao, T. In situ-grown heterostructured Co_3S_4/CNTs/C nanocomposites with a bridged structure for high-performance supercapacitors. *ACS. Omega.* **2021**, *6*, 33855-63. DOI PubMed PMC
35. Chen, Q.; Cai, D.; Zhan, H. Construction of reduced graphene oxide nanofibers and cobalt sulfide nanocomposite for pseudocapacitors with enhanced performance. *J. Alloys. Compd.* **2017**, *706*, 126-32. DOI